

# Temperature- and Bias-dependence of Magnetoresistance in Doped Manganite Thin Film Trilayer Junctions

J. Z. Sun and D. W. Abraham

IBM T. J. Watson Research Center, P. O. Box 218, Yorktown Heights, NY 10598

K. Roche and S. S. P. Parkin

IBM Almaden Research Center, 650 Harry Road, Almaden CA 95120

(June 26, 2021)

Thin film trilayer junction of  $\text{La}_{0.67}\text{Sr}_{0.33}\text{MnO}_3$  -  $\text{SrTiO}_3$  -  $\text{La}_{0.67}\text{Sr}_{0.33}\text{MnO}_3$  shows a factor of 9.7 change in resistance, in a magnetic field around 100 Oe at 14K. The junction magnetoresistance is bias and temperature dependent. The energy scales associated with bias and temperature dependence are an order of magnitude apart. The same set of energies also determine the bias and temperature dependence of the differential conductance of the junction. We discuss these results in terms of metallic cluster inclusions at the junction-barrier interface.

Large low-field magnetoresistance (MR) has been observed in trilayer thin film junctions of  $\text{La}_{0.67}\text{Sr}_{0.33}\text{MnO}_3/\text{SrTiO}_3/\text{La}_{0.67}\text{Sr}_{0.33}\text{MnO}_3$  [1–5]. The mechanism is yet to be fully understood. These manganites are expected to be half-metals [6,7] when ferromagnetic order is fully developed. Their low carrier concentration in the minority band makes its minority carrier prone to disorder-induced localization [7]. According to spin-dependent tunneling models [8–11], a half-metallic metal-insulator-metal junction would exhibit large, almost infinite MR. However, the observed bias- and temperature-dependence don't correspond to a clean metal-insulator-metal tunneling process. The junction resistance varies strongly with temperature, especially above 130K, indicating a barrier with high concentration of defects [2,4,5]. The MR disappears prematurely above 130K, well below the Curie temperature  $T_c = 360\text{K}$  of the electrodes. In addition, the junction MR is strongly bias-dependent when a bias-voltage of the order of 0.1V is applied.

Here we quantify the temperature- and bias-dependent magnetotransport properties of junctions made of  $\text{La}_{0.67}\text{Sr}_{0.33}\text{MnO}_3/\text{SrTiO}_3/\text{La}_{0.67}\text{Sr}_{0.33}\text{MnO}_3$  (LSMO/STO/LSMO) and  $\text{La}_{0.67}\text{Sr}_{0.33}\text{MnO}_3/\text{Al}_2\text{O}_3$ /Permalloy (LSMO/AO/Py) trilayers. A low-bias minimum develops in the differential conductance for temperatures below 120K, indicating the possible presence of a Coulomb gap. Two energy scales are present: first, an energy corresponding to the bias voltage for the suppression of MR. This energy happens to coincide with the bias level for the onset of a low-bias conductance minimum; secondly, an energy associated with the high-temperature suppression of MR, which happens to be identical to the temperature for the disappearance of the low-bias conductance minimum. We also show LSMO/STO/LSMO junctions with an order of magnitude change in resistance in 100 Oe, indicating that the intrinsic MR in these junctions is likely to be very large.

The fabrication process for LSMO/STO/LSMO junctions have been discussed in detail before [1,12,13]. The process for LSMO/AO/Py is similar. In both cases the base LSMO film is around  $500 \sim 600\text{\AA}$  thick. The top LSMO film is around  $400\text{\AA}$ . The LSMO films are grown epitaxially on  $\text{LaAlO}_3(100)$  or on  $\text{NdGaO}_3(110)$  substrates using laser ablation.

FIG. 1. An AFM image of a representative film surface, showing a peak-to-peak roughness around  $15\text{\AA}$ . An accompanying scanning electron micrograph is shown to the right for comparison.

The surface of these laser ablation-grown LSMO films are quite smooth. An example is shown in Fig.1, where an atomic force microscopy (AFM) image was taken on a single layer LSMO film,  $1000\text{\AA}$  thick, grown using the above mentioned deposition process on  $\text{NdGaO}_3(110)$  surface. The peak-to-peak surface roughness in this case is around  $15\text{\AA}$ , excluding laser particulates which has a typical density of around  $\sim 10^6/\text{cm}^2$ .

For LSMO/STO/LSMO junctions, the entire trilayer structure was made *in situ*. For LSMO/AO/Py trilayers, the film samples were transported to a different vacuum system after the deposition of LSMO. The wafer was first cleaned by exposure to 30sec of oxygen plasma. The  $\text{Al}_2\text{O}_3$  barrier layer was formed by sputter deposition of  $12\text{\AA}$  of aluminum, followed by 120sec plasma oxidation [14]. The Permalloy counter electrode was then sputter deposited,  $120\text{\AA}$  thick, in a process similar to that used in metallic magnetic tunneling junctions [14]. For both type of films the same photolithography process was used to define the current-perpendicular junction structure.

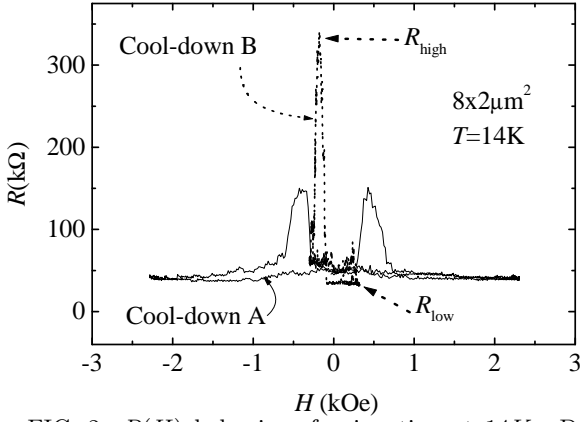


FIG. 2.  $R(H)$  behavior of a junction at 14K. Data are 10-trace averaged. Field was swept at  $0.13Hz$ . Junction bias was  $10nA$ . After cool-down A, a factor of 2 change in  $R$  was seen. A very large MR, of  $R_{high}/R_{low} = 9.7$  was seen at low sweeping amplitude of around  $100Oe$  during another cool-down(B).

An example of the dc junction resistance vs. applied field,  $R(H)$ , is shown in Fig.2. The junction pillar was  $8\mu m \times 2\mu m$  in size, sitting on a  $40\mu m$  wide base stripe, with its long axis perpendicular to the direction of the stripe. The magnetic field was applied parallel to the film surface along the long axis. The measurement temperature was 14K, and the junction was biased at  $10nA$ . From  $R(H)$  loops as these one defines a junction resistance  $R_{high}$ , corresponding to the resistive-high state of the junction, and a  $R_{low}$  for the resistive-low state.

The  $R(H)$  behavior is history dependent. After cool-down (A), a factor of 2 change in  $R$  was seen on the 10-trace averaged  $R(H)$ . During another cool-down (cool-down (B) in Fig.2), when the field sweep amplitude was first opened up from zero, a very large MR, of  $R_{high}/R_{low} = 9.7$ , was seen at low sweeping amplitude of around  $100Oe$ . These results highlight the importance the electrode's magnetic state has on junction transport properties. It is likely that the intrinsic MR in these structures is even larger, and that the actual MR one observed is still limited by the distribution of magnetic domains.

Fig.3 shows the temperature dependence of  $R_{high}$  and  $R_{low}$ . Both  $R_{high}$  and  $R_{low}$  are taken from 10-trace averaged  $R(H)$  loops. For  $T > 130K$ , they follow an  $\exp[(T_o/T)^{1/4}]$  scaling [3]. Below  $130K$ ,  $R_{high}$  and  $R_{low}$  branch apart, giving an MR that increases upon decreasing temperature. The noise in data is again a consequence of magnetic instabilities of the electrodes.

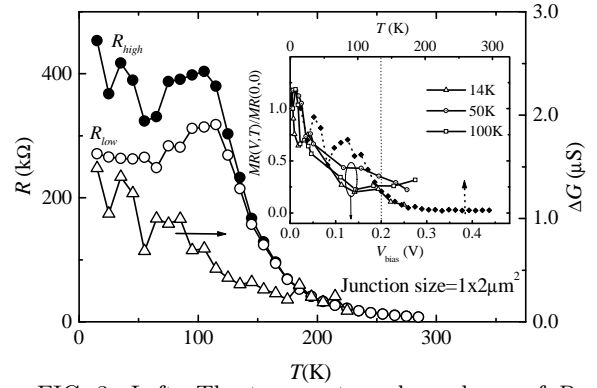


FIG. 3. Left: The temperature dependence of  $R_{high}$  and  $R_{low}$ . Right: conductance difference between  $R_{high}$  and  $R_{low}$  showing continuous decrease for  $T < 130K$ . Inset: Bottom axis, bias-dependence of the normalized MR (i.e.,  $MR(V,T)/MR(0,0)$ ) for three different temperatures. Although the magnitude of MR varies with temperature, its bias-dependence remained essentially temperature independent. Top axis: normalized MR vs. temperature.

Also shown in Fig.3 is the conductance difference  $\Delta G = \frac{1}{R_{low}} - \frac{1}{R_{high}}$  vs. temperature. A continuous decrease was seen of  $\Delta G(T)$  at the low temperature end, where  $R_{high}$  and  $R_{low}$  are only weakly temperature dependent. This rules out the parallel shunt mechanism [3] as an explanation for the decrease of MR in this temperature region, because parallel shunt from MR-inactive channels would have a constant  $\Delta G(T)$ .

The junction MR is bias-dependent. The inset of Fig.3 shows the bias-dependence of junction MR at several temperatures. The MR is suppressed to  $\sim 25\%$  of its low-bias value at a bias-voltage of  $0.2V$ . Although the magnitude of MR decreases rapidly with increasing  $T$ , the characteristic bias-dependence of which remained essentially temperature independent. Shown in the same plot is MR as a function of temperature. Here  $MR = \frac{R_{high} - R_{low}}{R_{low}}$ , all resistances are dc.

Data in Fig.3 inset reveal two energy scales. The first relates to the bias-voltage:  $E_b \sim 200meV$ . This corresponds to the bias level at which MR is suppressed. The second relates to the temperature:  $E_T \sim 130K = 11meV$ , corresponding to the temperature that suppresses MR. The two energy scales are an order of magnitude apart.

Fig.4(a) shows the evolution of the differential junction conductance  $\sigma_D = \frac{dJ}{dV}$  with temperature. The high temperature and high bias-voltage part of  $\sigma_D$  probably represents conduction via shallow defect states in the barrier [15] which we are not going to discuss. Instead, notice that for temperatures below  $120K$  ( $\sim E_T$ ), a conductance minimum develops for bias-voltages below  $200meV$  ( $\sim E_b$ ). Again,  $E_b$  and  $E_T$  show up as the energy scales associated with bias and temperature dependence.

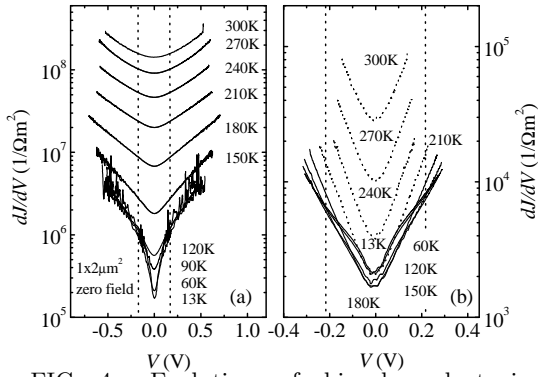


FIG. 4. Evolution of bias-dependent junction differential conductance with temperature. (a) For an LSMO/STO/LSMO junction. The two energy scales,  $E_b$  and  $E_T$  are again present. (b) Same measurement for an LSMO/AO/PyO junction, showing the same energy scales.

The development of a low-bias conductance minimum also occurs in LSMO/AO/Py junctions, as shown in Fig.4(b). Again, there is a characteristic temperature of  $T = 180K$  close to  $E_T$  observed before, and a characteristic voltage of  $200meV$  for low-bias conductance minimum, similar to the  $E_b$  of data in Fig.4(a).

The fact that both  $E_T$  and  $E_b$  are present for junctions made with different barrier and counter-electrodes suggest the mechanism(s) responsible for them are associated with the base electrode LSMO film, possibly with its interface at the barrier, rather than with the specifics of the barrier physics.

One mechanism that could produce conductance minimums over a wide range of bias conditions is metallic inclusions at the junction interface. The metallic inclusions, if small enough, will show a Coulomb gap in its low-bias conductance [16]. The conductance minimum in this case relates to the effective capacitance of the inclusion cluster, which is proportional to the cluster size, roughly speaking. Assuming the charging energy can be estimated as [17–19]  $E_c = \frac{e^2}{2C} = \frac{1}{8\pi\epsilon\epsilon_0} \left(\frac{e^2}{d}\right) F_o$ , where  $e$  is electron charge,  $C$  is the capacitance of the cluster,  $\epsilon$  the matrix dielectric constant,  $d$  the diameter of the cluster,  $F_o$  is a form factor that depends on the details of the local environment of the cluster and its distance to other conducting structures ( $F_o = 2$  for an isolated cluster), and assume  $\epsilon = 5$ ,  $F_o = 2$  (See [18] for estimate of  $F_o$ ), one gets  $d \approx 15\text{\AA}$ . Is it possible that there are metallic clusters at the LSMO surface of dimensions around  $15\text{\AA}$ ? Could these be related to the localization length of the spin-polarized carriers? these are open questions at present.

The conductance minimum from a single Coulomb gap is very sharp at low bias [16]. A distribution of  $E_c$  is likely to be present that could smear out the sharp low-bias cusp in the Coulomb gap's conductance, making it appear similar to the shape observed.

The hypothesis of a Coulomb gap explains the bias de-

pendent behavior, but it would not explain the temperature dependence. Since  $E_T$  is an order magnitude lower than  $E_b$ , some other mechanism(s) must be involved in suppressing the gap formation process for temperatures above  $E_T$ .

We wish to thank John Slonczewski, Bill Gallagher, Roger Koch, Arunava Gupta, Steve Brown, John Connolly at IBM Research Yorktown Heights; Xinwei Li, Yu Lu and Gang Xiao from Brown University for helpful discussions and for assistance at various stages of the experiment.

- 
- [1] J. Z. Sun, W. J. Gallagher, P. R. Duncombe, L. Krusin-Elbaum, R. A. Altman, A. Gupta, Y. Lu, G. Q. Gong, and G. Xiao, *Appl. Phys. Lett.* **69**, 3266 (1996).
  - [2] J. Z. Sun, L. Krusin-Elbaum, A. Gupta, G. Xiao, P. R. Duncombe, and S. S. P. Parkin, *IBM J. of Res. and Dev.* **42**, 89 (1998).
  - [3] J. Z. Sun, L. Krusin-Elbaum, P. R. Duncombe, A. Gupta, and R. B. Laibowitz, *Appl. Phys. Lett.* **70**, 1769 (1997).
  - [4] Y. Lu, X. W. Li, G. Q. Gong, G. Xiao, A. Gupta, P. Lecoeur, J. Z. Sun, Y. Y. Wang, and V. P. Dravid, *Phys. Rev. B* **54**, R8357 (1996).
  - [5] M. Viret, M. Drouet, J. Nassar, J. P. Contour, C. Feron, and A. Fert, *Europhysics Letters* **39**, 545 (1997).
  - [6] W. E. Pickett and D. J. Singh, *Phys. Rev. B* **53**, 1146 (1996).
  - [7] W. E. Pickett and D. J. Singh, *J. Magn. and Magn. Mat.* **172**, 237 (1997).
  - [8] J. Slonczewski, *IBM Technical Disclosure Bulletin* **19**, 2328 (1976).
  - [9] M. Julliere, *Phys. Lett.* **54A**, 225 (1975).
  - [10] J. C. Slonczewski, *Phys. Rev. B* **39**, 6995 (1989).
  - [11] A. M. Bratkovsky, *Phys. Rev. B* **56**, 2344 (1997).
  - [12] J. Z. Sun, L. Krusin-Elbaum, S. S. P. Parkin, and G. Xiao, *Appl. Phys. Lett.* **67**, 2726 (1995).
  - [13] J. Z. Sun, L. Krusin-Elbaum, A. Gupta, G. Xiao, and S. S. P. Parkin, *Appl. Phys. Lett.* **69**, 1002 (1996).
  - [14] W. J. Gallagher, S. S. P. Parkin, Y. Lu, X. P. Bian, A. Marley, R. A. Altman, S. A. Rishton, K. P. Roche, C. Jahnes, T. M. Shaw, and G. Xiao, *J. Appl. Phys.* **81**, 3741 (1996).
  - [15] Y. Xu, D. Ephron, and M. R. Beasley, *Phys. Rev. B* **52**, 2843 (1995).
  - [16] H. R. Zeller and I. Giaever, *Phys. Rev.* **181**, 789 (1969).
  - [17] J. S. Helman and B. Abeles, *Phys. Rev. Lett.* **37**, 1429 (1976).
  - [18] P. Sheng, B. Abeles, and Y. Arie, *Phys. Rev. Lett.* **31**, 44 (1973).
  - [19] P. Sheng, *Phil. Mag. B* **65**, 357 (1992).

This figure "fig1.jpg" is available in "jpg" format from:

<http://arxiv.org/ps/cond-mat/9807097v1>